Mapping of the Residues Involved in a Proposed β-Strand Located in the Ferric Enterobactin Receptor FepA Using Site-Directed Spin-Labeling[†]

Candice S. Klug, Wenyi Su, and Jimmy B. Feix*

Biophysics Research Institute, Medical College of Wisconsin, 8701 Watertown Plank Road, Milwaukee, Wisconsin 53226

Received May 27, 1997; Revised Manuscript Received August 13, 1997[⊗]

ABSTRACT: Electron paramagnetic resonance (EPR) site-directed spin-labeling (SDSL) has been used to characterize a proposed transmembrane β-strand of the *Escherichia coli* ferric enterobactin receptor, FepA. Each of nine consecutive residues was mutated to cysteine and subsequently labeled with the sulfhydryl-specific spin-label methanethiosulfonate (MTSL) and the purified protein reconstituted into liposomes. Continuous wave (CW) power saturation methods were used to determine exposure of the nitroxide side chains to a series of paramagnetic relaxation agents, including nickel acetylacetonate (NiAA), nickel ethylenediaminediacetate (NiEDDA), chromium oxalate (CROX), and molecular oxygen. The spin-label attached to Q245C, L247C, L249C, A251C, and Y253C had higher collision frequencies with molecular oxygen than with polar relaxation agents, indicating that these sites are exposed to the hydrophobic phase of the lipid bilayer. MTSL bound to residues S246C, E248C, E250C, and G252C had higher collision rates with the polar agents than with oxygen, suggesting that these sites are exposed to the aqueous channel. The alternating periodicity observed with the polar relaxation agents, NiAA and NiEDDA, and in opposite phase with oxygen, is consistent with β-sheet structure. Depth measurements, based on the reciprocal concentration gradients of NiEDDA and O_2 across the bilayer and calibrated for our system with phosphatidylcholine spin-labels, indicated that L249C was nearest the center of the bilayer and that Q245C and Y253C were located just below the bilayer surface in opposite leaflets of the membrane. Thus, we conclude that this approach, through mapping of individual residues, has the capability of defining β-sheet secondary structure.

The outer membrane of Gram-negative bacteria is an important barrier to toxins, antibiotics, and other noxious agents often found in the bacterial environment. The existence of this protective barrier also gives rise to the need for proteins that can facilitate the uptake of required nutrients and elimination of waste products (Nikaido, 1992; Nikaido & Saier, 1992). Outer membrane (OM) proteins include porins such as OmpF and PhoE, low-specificity diffusion channels that allow passage of solutes less than about 600 Da, and LamB, which has moderate specificity for maltosides. In recent years, crystal structures have been determined for OmpF and PhoE (Cowan *et al.,* 1992), the general porins of *Rhodobacter capsulatus* (Weiss *et al.,* 1991; Przybylski *et al.,* 1996) and *Rhodopseudomonas blastica* (Kreusch *et al.,* 1994), and LamB (Schirmer *et al.,* 1995). Common structural features of these OM proteins are a transmembrane domain composed of a series of antiparallel β-strands arranged in a β-barrel configuration and surface loops that act to impart specificity or to restrict access to the underlying channel.

An additional group of OM proteins are the ligand-gated porins, high-specificity receptors that actively transport their cognate ligands and require interaction with the inner membrane protein, TonB. These include the vitamin B_{12} receptor, BtuB (Kadner, 1990; Postle, 1990), receptors for a variety of iron complexes (siderophores) such as the ferrichrome receptor, FhuA (Koebnik & Braun, 1993), and the ferric enterobactin receptor, FepA (Hollifield & Neilands, 1978). No solved crystal structure has yet been reported for a TonB-dependent OM protein.

FepA is an 81 kDa TonB-dependent integral membrane protein responsible for transporting the siderophore, ferric enterobactin, across the outer membrane of Gram-negative bacteria. Based on immunochemical studies, hydropathy analysis, and analogy to other OM proteins, FepA has been predicted to form a β-barrel structure containing 29 antiparallel β-strands (Murphy *et al.,* 1990). A large hydrophilic loop, centrally located in the primary structure, has been shown to contain the ligand-binding domain and to maintain the channel in a closed conformation. Deletion of this central loop converts FepA from a high-affinity ligand-gated channel to an open diffusion pore (Rutz *et al.,* 1992; Liu *et al.,* 1993).

In this study, we utilize the electron paramagnetic resonance (EPR)[1] site-directed spin-labeling (SDSL) approach to examine the secondary structure and membrane localization of one of the proposed transmembrane strands of FepA reconstituted into liposomes. SDSL is a valuable technique

[†] Supported by National Institutes of Health Grants GM51339, GM22923, and RR01008.

* Author to whom correspondence should be addressed at the Biophysics Research Institute, Medical College of Wisconsin, 8701 Watertown Plank Rd., Milwaukee, WI 53226. FAX: 414-456-6512. E-mail: jfeix@post.its.mcw.edu.

[⊗] Abstract published in *Advance ACS Abstracts,* October 1, 1997.

[1] Abbreviations: EPR, electron paramagnetic resonance; CROX, potassium tris(oxalato)chromate (or chromium oxalate); NiAA, nickel(II) acetylacetonate; NiEDDA, nickel(II)−ethylenediaminediacetate complex; MTSL, methanethiosulfonate spin-label; MOPS, 3-(*N*-morpholino)propanesulfonic acid; PCR, polymerase chain reaction; eggPC, egg L-α-phosphatidylcholine; POPG, 1-palmitoyl-2-oleoylphosphatidylglycerol; LB, Luria broth; DTT, dithiothreitol; DPPH, 2,2-diphenyl-1-picrylhydrazyl.

S0006-2960(97)01232-4 CCC: $14.00

Scheme 1: Chemistry of Site-Specific Spin-Labeling with MTSL[a]

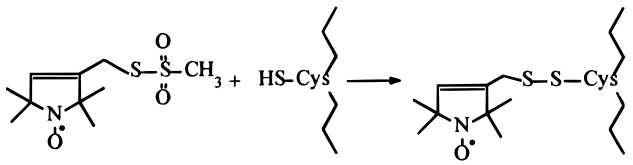

[a] The methanethiosulfonate spin-label reacts exclusively with the free sulfydryl group on the introduced cysteine residue.

which can provide detailed information on the environment and location of an individual residue within a protein structure (Hubbell & Altenbach, 1994; Liu *et al.*, 1994; Klug *et al.*, 1995; Mchaourab *et al.*, 1997). This is especially useful when studying large membrane proteins such as FepA which are not amenable to analysis by NMR techniques and which lack a solved crystal structure. Using site-directed mutagenesis, a cysteine is inserted in place of the residue of interest and subsequently modified with a sulfhydryl-specific spin-label (Scheme 1). The motional dynamics of the attached spin-label and its accessibility to various paramagnetic reagents provide insight into the local structure and conformational interactions at the labeled site. Using this method, we have investigated nine consecutive residues located in a proposed transmembrane segment near the active site loop, characterizing each by power saturation depth measurements. Our results confirm that these residues adopt a β-strand secondary structure spanning the lipid bilayer, with alternate residues facing the lipid alkyl chains and the aqueous interior of the channel. Additionally, strong tertiary interactions observed for the extracellular half of the strand imply strand−loop interactions that may be significant in ligand recognition or transport.

MATERIALS AND METHODS

Site-Directed Mutagenesis and Protein Purification. Single cysteine substitutions were made using the four-primer method and overlap−extension PCR with the wild-type FepA gene expressed in plasmid pITS449 (Armstrong *et al.*, 1990) as the template. Primers of 18−20 deoxynucleotides were from Operon (Alameda, CA). Mutations were verified by the dideoxynucleotide sequencing method using the Thermo Sequenase kit from Amersham International (Buckinghamshire, England). Each mutant was transformed into *E. coli* RWB18-60 for expression, and protein was purified as described previously (Neihardt *et al.*, 1974; Fiss *et al.*, 1982; Klug *et al.*, 1995).

Colicin Killing Assay. A total of 10^7 cells taken from a 2 mL overnight culture were added to 2 mL of top agar (7 g/L) containing either no colicin B or a titer sufficient to give complete killing in wild type, plated onto base agar (15g/L), and incubated overnight at 37 °C. A bacterial lawn was observed on the plates containing no colicin B, and susceptibility to the toxin was indicated by the absence of colonies on the plates containing colicin B. RWB18-60 (Leong & Neilands, 1976) and KDF541/pITS449 (Armstrong *et al.*, 1990) were plated as colicin B-resistant and sensitive controls, respectively.

Ferric Enterobactin Growth Assay. Purified enterobactin was reconstituted with iron by incubation with $FeCl_3$ and purified on a Sephadex LH-20 column (Murphy *et al.*, 1990). Purity was assessed by examining the absorbance ratio at 395 nm/495 nm, and concentration was determined from the absorption at 495 nm using an extinction coefficient of 5.6 mM^{-1} cm^{-1}. In order to test each mutant for ferric enterobactin uptake, a sterile filter disk (6 mm in diameter) containing 2−3 nmol of ferric enterobactin was added to the center of a 45 mm plate containing 2 mL of LB agar (15 g/L), 10^7 cells (from a 2 mL overnight culture), 0.1 mg of ampicillin, and 0.1 mM apoferrichrome. Plates were incubated at 37 °C overnight, and uptake was determined by the appearance of a growth halo surrounding the disk. KDF541/pITS449 (expressing plasmid-encoded wild-type FepA in a *fepA* background) with and without added ferric enterobactin was used as a positive and negative control, respectively.

Spin-Labeling. The purified protein was spin-labeled at the introduced cysteine residue with a 10-fold molar excess of the sulfhydryl-specific spin-label (1-oxy-2,2,5,5-tetramethylpyrrolidine-3-yl)methyl methanethiosulfonate (MTSL, Reanal, Budapest, Hungary) overnight at 4 °C. It has been shown previously that the two native cysteine residues are disulfide linked and will not label without prior treatment with a thiol reducing agent such as DTT (Liu *et al.*, 1994). Excess spin-label was removed by extensive dialysis followed by precipitation with 2 volumes of ice-cold ethanol.

Liposome Reconstitution and Sample Preparation. Liposomes were prepared by drying a chloroform solution containing 2 μmol of egg PC and 0.4 μmol of POPG under a stream of nitrogen and placing in a vacuum desiccator overnight. Purified spin-labeled protein (3 nmol) was resuspended in distilled water and added to the thin film of lipids. This suspension was then dried under a stream of nitrogen and placed in a vacuum desiccator for approximately 1 h. The lipid−protein film was resuspended in 20 mM MOPS, pH 7.2, containing CROX, NiAA, or NiEDDA as desired and incubated at 37 °C before being inserted into sample tubes. This method provides a uniform distribution of the appropriate broadening reagents on both sides of the bilayer in all regions of the multilamellar vesicles. The paramagnetic broadening reagents CROX [potassium tris(oxalato)chromate] and NiAA [nickel(II) acetylacetonate] were from Aldrich Chemical Co. (Milwaukee, WI). NiEDDA [nickel(II) ethylenediamine-*N*,*N*′-diacetic acid] was a gift from Dr. H. Mchaourab.

Electron Paramagnetic Resonance. EPR spectroscopy was performed on a Varian E-102 Century series X-band spectrometer (Varian Associates Inc., Palo Alto, CA) equipped with a loop−gap resonator (two loop−one gap; Froncisz & Hyde, 1982) using the VIKING software package for data collection and SUMSPC92 for data analysis (National Biomedical ESR Center, Milwaukee, WI). Samples were run in a gas-permeable TPX capillary (Popp & Hyde, 1981). Spectra were recorded using 1 mW incident microwave power and a modulation amplitude of 1.0 G. Power saturation experiments were carried out using a 1.25G modulation amplitude and varying microwave powers (typically 0.1−36 mW). During saturation experiments, the sample in the TPX capillary tube was purged with a continuous stream of either nitrogen or 20% oxygen (air). The peak-to-peak intensity of the first-derivative $m_I = 0$ resonance line (A) was measured and plotted against the square root of the incident microwave power. These data points were then fit, using Enzfitter (Elsevier-Biosoft, Cambridge, U.K.), to the equation:

$$A = IP^{1/2}[1 + (2^{1/\epsilon} - 1)P/P_{1/2}]^{-\epsilon} \quad (1)$$

as described by Altenbach *et al*. (1994), where I is a scaling factor, ϵ is a homogeneity factor, P is the incident microwave power, and $P_{1/2}$, the half-saturation parameter, is the microwave power at which the observed intensity of the first-derivative center line is half that which would be observed in the absence of saturation. In order to characterize accessibility for each mutant, power saturation data were obtained under several different conditions: under nitrogen gas, under air (20% oxygen), and in the presence of 20 mM CROX, 20 mM NiAA, or 200 mM NiEDDA under nitrogen. From these data, $\Delta P_{1/2}$ values were calculated by subtracting the $P_{1/2}$ value in the absence of a paramagnetic broadening reagent (under nitrogen gas) from the $P_{1/2}$ value in the presence of a paramagnetic broadening reagent (oxygen, CROX, NiAA, or NiEDDA). In addition, dimensionless Π values, which are normalized to correct for differences in T_{2e} and variabilities between resonators, were calculated using the equation:

$$\Pi = [\Delta P_{1/2}/\Delta H]/[P_{1/2}(\mathrm{DPPH})/\Delta H(\mathrm{DPPH})] \quad (2)$$

(Farahbakhsh *et al.*, 1992) where ΔH is the peak-to-peak first-derivative center line width and $P_{1/2}$(DPPH) and ΔH(DPPH) are the half-saturation power and the peak-to-peak width of a DPPH (2,2-diphenyl-1-picrylhydrazyl) standard, respectively. A Φ value was then calculated from the equation:

$$\Phi = \ln[\Delta P_{1/2}(\mathrm{O_2})/\Delta P_{1/2}(\mathrm{NiEDDA})] \quad (3)$$

(Altenbach *et al.*, 1994), and the depth (Å) of the attached spin-label exposed to the lipid bilayer was calculated according to the equation:

$$\text{depth (Å)} = 3.56\Phi + 3.62 \quad (4)$$

The above bilayer depth calibration equation was determined using phosphatidylcholine spin-labels (PCSLs) integrated into liposomes containing unlabeled FepA. Φ values for 5-, 7-, 10-, and 12-PCSL were measured and plotted against known depths of the spin-labels (Dalton *et al.*, 1987). Equation 4 was derived from linear regression analysis of the line passing through the plotted experimental points. A similar calibration was obtained using PCSLs in the presence of 20 mM NiAA. Doxylstearate spin-labels also show a linear dependence on Φ (data not shown).

RESULTS

A portion of the FepA structural model adapted from that proposed by Murphy *et al.* (1990) is shown in Figure 1. This model is based on immunochemical and antibody binding studies for many of the extracellular loops and on hydrophobicity calculations for the β-strands. The strand in which the cysteine mutations are located (Q245−Y253) is adjacent to the large extracellular loop containing the active site. Our study is the first to begin resolving the predicted model and proving the β-barrel proposal correct.

Colicin B and Ferric Enterobactin Effects. To assess the functional integrity of the mutant FepA receptors, we examined each for the ability to support growth under iron-limited conditions and for susceptibility to colicin B. Each of the mutants sustained ferric enterobactin-dependent growth

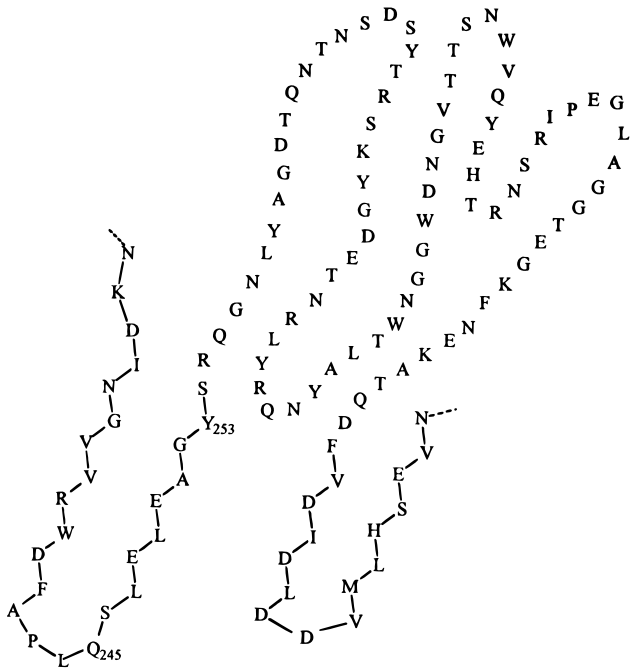

FIGURE 1: Model [adapted from that proposed by Murphy *et al.* (1990)] for the region of FepA surrounding the cysteine mutations (Q245−Y253) studied in this paper. Putative β-strands 8−11 (left to right) are shown along with the large extracellular ligand binding domain.

at levels similar to wild-type. However, Y253C was completely resistant to colicin B killing, and S246C was only partially susceptible to the toxin while the rest were fully susceptible to colicin B killing. The differentiation between ferric enterobactin and colicin B transport is somewhat rare, but has been reported previously (Armstrong *et al.*, 1990). Further studies to examine the basis of Y253C and S246C resistance are in progress. Nonetheless, these studies demonstrate that these FepA mutants containing specifically introduced cysteine residues bind and transport the native ferric enterobactin ligand, and furthermore indicate that the required interaction with TonB remains intact.

EPR Spectra. The EPR spectrum of each MTSL-labeled FepA mutant in liposomes is shown in Figure 2. With the exception of S246C, the nitroxide side chain is fairly strongly immobilized for each of the MTSL-labeled mutants, with $2T_{\parallel}'$ values between 62 and 65 G, where $2T_{\parallel}'$ is the separation between the outer hyperfine extrema (Hubbell & McConnell, 1971). In addition, all the mutants appear to contain two components in the low-field region.

Power Saturation Results. Continuous wave (CW) power saturation has proven to be a simple and convenient method to examine the accessibility of sites labeled with a nitroxide spin-label to aqueous and hydrophobic molecules (Hubbell & Altenbach, 1994). Collision of a spin-label with a fast-relaxing, paramagnetic broadening reagent enhances the spin−lattice relaxation rate of the nitroxide, increasing the power necessary for its saturation. This increase in power required for saturation ($\Delta P_{1/2}$) is directly proportional to the collision rate of the nitroxide with the paramagnetic broadening reagent, thus reflecting the environment surrounding the spin-label (Altenbach *et al.*, 1989). For spin-labels immersed in a lipid bilayer, the reciprocal concentration gradients of molecular oxygen and neutral, polar nickel complexes such as NiAA and NiEDDA, with oxygen concentration increasing as the environment becomes increasingly nonpolar and the

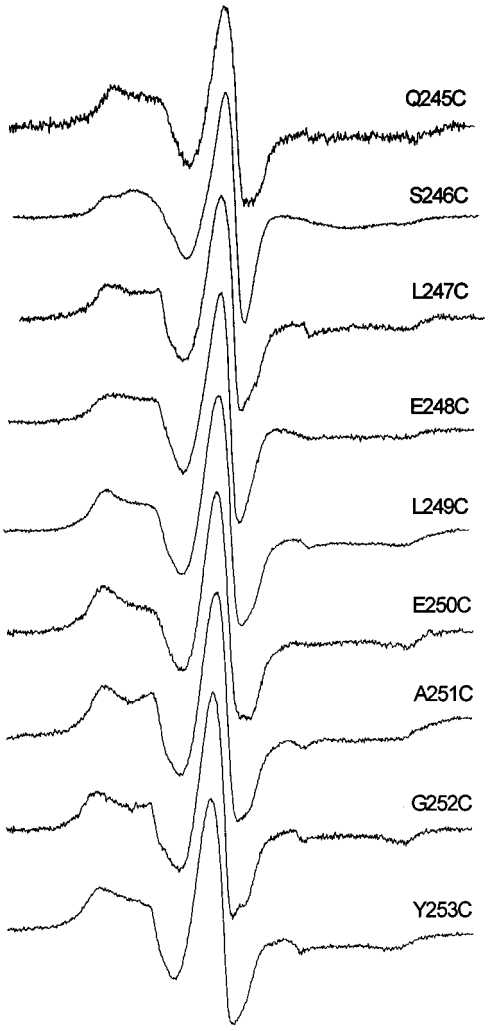

FIGURE 2: CW X-band EPR spectra of MTSL-labeled FepA mutants reconstituted into liposomes. All spectra were recorded with a 100 G scan width.

nickel complexes showing the opposite trend, allow estimation of the depth of the label in the membrane (Altenbach *et al.*, 1994). Chromium oxalate (CROX), a negatively charged molecule restricted to the aqueous phase, can also be used to probe accessibility (Altenbach *et al.*, 1989).

Results obtained from the power saturation experiments are summarized in Table 1. Depth values were not calculated for residues S246C, E248C, E250C, and G252C, as these residues appear to be located within the aqueous channel and are therefore not exposed to the oxygen and nickel gradients found within the bilayer. The Φ values and depth measurements found in Table 1 are based on the NiEDDA data while the NiAA data are included for qualitative comparison. The higher NiEDDA concentration (200 mM) is necessary in order for sufficient amounts of the complex to partition into the membrane to alter $P_{1/2}$ (Altenbach *et al.*, 1994).

The variation in both oxygen and NiEDDA accessibilities with label position show a striking biphasic periodicity (Figure 3). For the odd-numbered residues, Q245C, L247C, L249C, A251C, and Y253C, the attached MTSL side chain consistently has a higher accessibility to oxygen than to the nickel complexes, indicative of exposure to the hydrophobic alkyl chains of the lipid bilayer. In contrast, the even-numbered mutants do not appear to be exposed to the lipid phase of the bilayer (Table 1 and Figure 3). S246C is the most accessible to the aqueous reagents and sees very little oxygen, strongly indicating an aqueous environment which would be expected for a location at the inside base of the aqueous channel (see Discussion). Similarly, E248C interacts significantly more strongly with the nickel complexes than with oxygen and also shows strong interaction with CROX (Table 1), all of which indicate exposure to the aqueous phase. Unexpectedly, the next two consecutive channel-exposed residues, E250C and G252C, show low exposure to all of the relaxation agents used, including the polar reagents.

Combining the results of the two sets of residues and plotting their accessibilities to oxygen and NiEDDA leads to the conclusion that these residues do in fact comprise a β-strand. Figure 3 clearly indicates the alternating periodicity in both oxygen and NiEDDA accessibility parameters. A periodicity of 2.0 is unequivocally consistent with β-sheet secondary structure.

To assess the relative depths of the lipid exposed residues in the membrane bilayer, the ratio of accessibilities to oxygen and NiEDDA (see eq 3) was examined (Figure 4). L249C and A251C have the highest O_2:NiEDDA ratios (i.e., e^{Φ}), with depths calculated at 15.2 and 11.1 Å from the polar head groups, respectively (Table 1). Q245C interacts with relatively more NiEDDA, but still has a higher collision rate with oxygen than with either NiEDDA or CROX, placing it in the bilayer close to the membrane surface at a calculated depth of 5.1 Å. L247C is accessible to slightly less nickel and more oxygen, placing it deeper into the membrane at a calculated depth of 8.4 Å. Similarly, the high comparative interaction of Y253C with oxygen and intermediate interactions with CROX and NiEDDA suggest a depth of 7.7 Å. Taken together, the pattern observed in Figure 4 clearly indicates that this stretch of amino acids spans the membrane, with Q245 and Y253 near the lipid glycerol moiety in opposite leaflets and L249 nearest the center of the bilayer (Figure 5). In addition, the average separation of 6.3 Å between odd numbered residues is in good agreement with the separation of 6.8 Å in an ideal β-sheet (see Discussion).

DISCUSSION

In this study, we have utilized SDSL to map the location and local secondary structure of a proposed transmembrane β-strand in the ferric enterobactin receptor. Although this approach has proven quite valuable in examining the structure, tertiary interactions, and conformational dynamics of transmembrane α-helices (Altenbach *et al.*, 1989, 1990, 1994; Farahbakhsh *et al.*, 1992), this is the first report of such characterization for a transmembrane β-strand. In the present study, variation in CW power saturation parameters in the presence of both oxygen and polar nickel complexes as a function of spin-label position gave a well-defined alternating periodicity (Figure 3). This alternating periodicity is characteristic of β-sheet secondary structure, as observed previously with the soluble cellular retinol binding protein (Hubbell *et al.*, 1996).

Taken alone, the Π dependence shown in Figure 3 does not distinguish between a β-strand oriented along the bilayer normal and one that lies parallel to the membrane surface. However, examination of bilayer depths (Table 1) and the associated depth parameter, Φ (Figure 4), does indicate that

Table 1: Accessibility Parameters and Depth Calculations[a]

mutant	$\Delta P_{1/2}(O_2)$[b]	$\Delta P_{1/2}$(CROX)	$\Delta P_{1/2}$(NiAA)	$\Delta P_{1/2}$(NiEDDA)	Φ	depth (Å)
Q245C	2.46	0.92	1.62	1.61	0.42	5.1
S246C	1.47	3.77	>20[c]	>20[c]		
L247C	2.99	1.31	1.07	0.77	1.36	8.4
E248C	2.22	2.97	3.76	4.05	−0.60	
L249C	2.61	0.46	0.56	0.10	3.30	15.2
E250C	2.16	−0.05	0.15	0.97	0.80	
A251C	2.28	0.19	1.10	0.28	2.11	11.1
G252C	1.36	0.31	0.73	0.87	0.62	
Y253C	2.08	0.53	1.23	0.66	1.15	7.7

[a] Power saturation parameters reflecting accessibility and bilayer depth for spin-labeled FepA cysteine mutants in liposomes. [b] $\Delta P_{1/2}$ parameters were obtained in the presence of air (20% oxygen), 20 mM CROX, 20 mM NiAA, or 200 mM NiEDDA, as described in the text. Φ values and subsequent depth measurements were calculated from eqs 3 and 4 (see text). [c] S246C-MTSL did not saturate in the presence of either 20 mM NiAA or 200 mM NiEDDA.

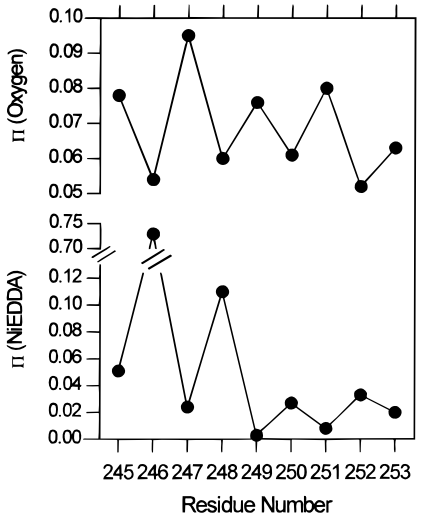

FIGURE 3: Variation in the accessibility parameter Π for oxygen and NiEDDA as a function of spin-label position. An alternating periodicity is observed for both relaxation agents, indicative of β-sheet secondary structure. Sites with relatively high $\Pi(O_2)$ and low Π(NiEDDA) values are exposed to the lipid phase of the membrane, while those with high Π(NiEDDA) and low $\Pi(O_2)$ values are oriented toward the aqueous channel.

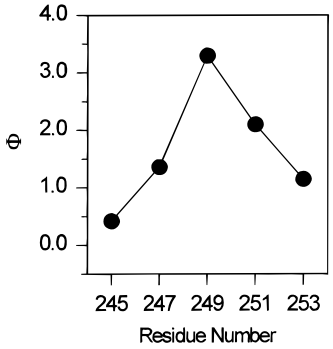

FIGURE 4: Variation in the depth parameter Φ with spin-label position for lipid-exposed mutants. Φ values, derived from relative interactions of the given spin-label sites with O_2 and NiEDDA (see text), increase with increasing depth into the bilayer.

this strand spans the bilayer. Orientation along the bilayer surface is not compatible with the depth separation between nitroxides attached to E248C and L249C that would be indicated by their relative Φ values, and would also require the strand to be sharply bent around residue 249. The observed depth dependence is much better fit by a transmembrane orientation of the strand, in agreement with what is known about other bacterial outer membrane proteins.

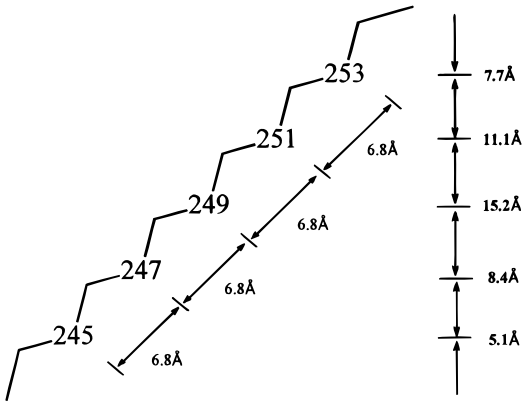

FIGURE 5: Visual model of the transmembrane β-strand encompassing residues Q245 through Y253. Depth measurement data collected by EPR power saturation experiments are shown on the right, and model antiparallel β-sheet parameters (6.8 Å separation between alternate residues) are shown on the left.

The MTSL side chain bound to residues E250C and G252C was remarkably inaccessible to both polar and nonpolar relaxation agents (Figure 3 and Table 1), in sharp contrast to sites S246C and E248C located on the opposite side of the channel. By analogy to porins for which crystal structures have been solved, this restriction could possibly be due to structural interactions with surface loops. In the LamB maltoporin, three of the nine surface loops fold back into the channel along with a surface loop from an adjacent subunit in the functional trimer (Schirmer *et al.*, 1995). For the *E. coli* porins PhoE and OmpF, one large surface loop in particular folds back into the aqueous channel, forming a constriction that determines the exclusion limit for solute diffusion through the pore (Cowan *et al.*, 1992). This structural characteristic is also observed for the general porin from *Rhodobacter capsulatus* (Weiss *et al.*, 1991). Thus, the steric hindrance observed at E250 and G252 may arise from interaction with one of the surface loops of FepA, in particular, the large extracellular loop proposed to include residues 256−336 that contains the ligand binding site. Guanidine denaturation studies have shown that the spin-label at E250C becomes freely mobile at concentrations of denaturant that produce unfolding of this surface loop, whereas sites on the hydrophobic side of the barrel (L247C and L249C) do not (Klug *et al.*, 1997). Whether or not there are specific structural interactions involving surface loops and the particular β-strand we have mapped, or simply reduced accessibility due to a more general steric hindrance arising from occlusion of the channel by surface loops, is

not known. Based on the above analogies combined with our spectroscopic studies, we suggest that the ligand-binding surface loop folds back into the aqueous channel where it forms structural interactions that may have obvious functional importance in ligand recognition and transport.

In addition, S246C is expected to be located at the base of the channel as part of the β-strand studied. This conclusion arises due to its high accessibility to aqueous reagents and to the depths measured for the two adjacent residues Q245C and L247C. Since both Q245 and L247 have been shown to be lipid-exposed and are located at depths of 5.1 Å and 8.4 Å, respectively, S246 is then positioned near the inside base of the channel on the β-strand. Although the high accessibility to the aqueous paramagnetic broadening reagents alone may indicate that this residue is located in a β-turn, the above depth measurements along with the fact that residue 243 is a proline (see Figure 1) make it unlikely L247 ends one strand and Q245 begins another with S246 the only residue comprising the β-turn between strands.

Since the lipid composition of our membranes differs from that studied by Altenbach *et al.* (1994), it was important to develop a calibration curve characteristic of our specific system. Wild-type (unlabeled) FepA was included in the system used for calibration since membrane proteins can influence the transmembrane dipole potential and hence the distribution of polar relaxation agents. Originally, the depth measurements were calculated using 20 mM NiAA. However, using NiAA, we observed inconsistencies with the two mutants nearest the surface (Q245C and Y253C). Because the presence of charged species is known to complicate accessibility measurements (Altenbach *et al.*, 1994), 200 mM NiEDDA was used as a more stable alternative and has been proven just as useful in these types of studies (Altenbach *et al.*, 1994, 1996; Yu *et al.*, 1994). Bilayer depths calculated from O_2:NiAA ratios (based on a separate calibration curve determined for NiAA) were slightly greater than those obtained with NiEDDA, but followed the same trend.

The depth measurements for each residue are assumed to be indicative of the depth of the residue at approximately the C_α, inferring the nitroxide is in an extended position perpendicular to the β-strand backbone. This is certainly an approximation. The nitroxide could also be positioned against the protein backbone, as assumed by molecular modeling (Mchaourab *et al.*, 1997). The EPR spectra of our MTSL-labeled mutants (Figure 2) all contain indications of more than one spectral component, reflecting the ability of the side chain to adopt various conformations relative to the protein backbone. These conformations may vary according to site, as defined by interactions with closely neighboring side chains. Consequently, calculated depths in the bilayer should be taken as approximations in which some deviation from the C_α position is not unexpected. Nonetheless, the general trend in Φ values across the β-strand (Figure 4) clearly provides a well-defined model of relative depths in the bilayer.

Our results indicate an average of 6.3 Å between alternate residues, assuming the center of the bilayer is 19 Å below the lipid phosphate groups based on comparison with crystal structure data obtained for the related protein LamB (Schirmer *et al.*, 1995). Although we presume that the center of the bilayer lies between 249 and 251, it should be noted that the calculated average separation does not depend on which residue is closest to the bilayer center. It is assumed, since the distances are less than the model 6.8 Å value, that the strands comprising this β-barrel structure are at an angle to the bilayer normal. This is entirely expected given the nature of β-barrel structures. Based on these measurements, we can begin to predict the tilt angle of the β-strands and the possible total number of strands found in FepA. Using the distance measurements between each residue as measured by power saturation experiments, it is possible to obtain the angle of tilt from the bilayer normal, α. The tilt of the β-strands can be determined using the equation $\cos \alpha = a/b$ where a is the average experimentally determined distance between residues perpendicular to the bilayer normal and b is the distance between each residue along the tilted strand which is assumed to be 6.8 Å, the translation used in model β-strands. Based on $a = 6.3$ Å and $b = 6.8$ Å, the tilt angle (α) for this particular β-strand is 22°, lower than the average angle (35°−50°) observed in crystallized 16-stranded porins (Cowan *et al.*, 1992; Kreusch *et al.*, 1994). However, FepA is much larger than these porins (723 amino acids vs less than 350), contains a larger diffusion channel (Liu *et al.*, 1993), and is proposed to have a greater number of strands (29) forming the barrel (Murphy *et al.*, 1990). Consequently, the tilt of individual strands may be less extreme.

Further extrapolation of the above data can lead to a prediction of the diameter of the barrel. The geometric characteristics of model β-barrels can be described by

$$R = [(3.3S)^2 + (4.4n)^2]^{1/2}/[(2n) \sin (180/n)] \quad (5)$$

and

$$\tan \alpha = 0.75S/n \quad (6)$$

(Chothia & Murzin, 1993) where R is the mean radial distance of the barrel, S is the shear number or measure of the stagger of the β-strand (see aforementioned paper for illustrated description), and n is the total number of strands in the β-barrel. Using $n = 29$, as predicted in the model by Murphy *et al.* (1990), and $\alpha = 22°$, as determined above, the radius of the barrel becomes 22 Å. Analysis of the crystal structure of LamB (18 strands) using Molw PDB Viewer (Molecular Imaging, San Diego, CA) suggested a barrel radius of nearly 20 Å, making the 22 Å estimate not unreasonable. Again, it should be noted that there is a great deal of variability in the tilt angle even between strands within a single porin; thus, the strand we have characterized in this study may not be representative of the average tilt angle. Further analysis of neighboring strands and SDSL measurements of distances between strands should provide a more accurate understanding of the β-barrel geometry of FepA.

In conclusion, we have studied nine consecutive residues located on a proposed β-strand near the active site of FepA and shown, using site-directed spin-labeling and EPR power saturation techniques, that they are involved in β-sheet secondary structure, as indicated by a well-defined periodicity of 2.0.

ACKNOWLEDGMENT

We thank Dr. Tim Herman for his generous efforts toward teaching us the art of site-directed mutagenesis. We also thank Dr. Hassane Mchaourab for several helpful discussions.

REFERENCES

Altenbach, C., Flitsch, S. L., Khorana, H. G., & Hubbell, W. L. (1989) *Biochemistry 28,* 7806−7812.

Altenbach, C., Marti, T., Khorana, H. G., & Hubbell, W. L. (1990) *Science 248*, 1088−1092.
Altenbach, C., Greenhalgh, D. A., Khorana, H. G., & Hubbell, W. L. (1994) *Proc. Natl. Acad. Sci. U.S.A. 91*, 1667−1671.
Armstrong, S. K., Francis, C. L., & McIntosh, M. A. (1990) *J. Biol. Chem. 265*, 14536−14543.
Chothia, C., & Murzin, A. G. (1993) *Structure 1*, 217−222.
Cowan, S. W., Schirmer, T., Rummel, G., Steiert, M., Ghosh, R., Pauptit, R. A., Jansonius, J. N., & Rosenbusch, J. P. (1992) *Nature 358*, 727−733.
Dalton, L. A., McINtyre, J. O., & Fleischer, S. (1987) *Biochemistry 26*, 2117−2130.
Farahbakhsh, Z. T., Altenbach, C., & Hubbell, W. L. (1992) *Photochem. Photobiol. 56*, 1019−1033.
Fiss, E. H., Stanley-Samuelson, P., & Neilands, J. B. (1982) *Biochemistry 21*, 4517−4522.
Froncisz, W., & Hyde, J. S. (1982) *J. Magn. Reson. 47*, 515−521.
Hollifield, W. C., Jr., & Neilands, J. B. (1978) *Biochemistry 17*, 1922−1928.
Hubbell, W. L., & McConnell, H. M. (1971) *J. Am. Chem. Soc. 93*, 314−326.
Hubbell, W. L., & Altenbach, C. (1994) *Curr. Opin. Struct. Biol. 4*, 566−573.
Hubbell, W. L., Mchaourab, H. S., Altenbach, C., & Lietzow, M. A. (1996) *Structure 4*, 779−783.
Kadner, R. J. (1990) *Mol. Microbiol. 4*, 2027−2033.
Klug, C. S., Su, W., Liu, J., Klebba, P. E., & Feix, J. B. (1995) *Biochemistry 34*, 14230−14236.
Klug, C. S., Su, W., & Feix, J. B. (1997) *Biophys. J. 72*, A205.
Koebnik, R., & Braun, V. (1993) *J. Bacteriol. 175*, 826−839.
Kreusch, A., Neubuser, A., Schiltz, E., Weckesser, J., & Schultz, G. E. (1994) *Protein Sci. 3*, 58−63.
Leong, J., & Neilands, J. B. (1976) *J. Bacteriol. 126*, 823−830.
Liu, J., Rutz, J. M., Feix, J. B., & Klebba, P. E. (1993) *Proc. Natl. Acad. Sci. U.S.A. 90*, 10653−10657.
Liu, J., Rutz, J. M., Klebba, P. E., & Feix, J. B. (1994) *Biochemistry 33*, 13274−13283.
Mchaourab, H. M., Oh, K. J., Fang, C. J., & Hubbell, W. L. (1997) *Biochemistry 36*, 307−316.
Murphy, C. K., Kalve, V. I., & Klebba, P. E. (1990) *J. Bacteriol. 172*, 2736−2746.
Neihardt, F. C., Bloch, P. L., & Smith, D. F. (1974) *J. Bacteriol. 119*, 736−747.
Nikaido, H. (1992) *Mol. Microbiol. 6*, 435−442.
Nikaido, H., & Saier, M. H., Jr. (1992) *Science 258*, 936−942.
Popp, C. A., & Hyde, J. S. (1981) *J. Magn. Reson. 43*, 249−258.
Postle, K. (1990) *Mol. Microbiol. 4*, 2019−2025.
Przybylski, M., Glocker, M. O., Nestel, U., Schnaible, V., Bluggel, M., Diederichs, K., Weckesser, J., Schad, M., Schmid, A., Welte, W., & Benz, R. (1996) *Protein Sci. 5*, 1477−1489.
Rutz, J. M., Liu, J., Lyons, J. A., Goranson, J., Armstrong, S. A., McIntosh, M. A., Feix, J. B., & Klebba, P. E. (1992) *Science 258*, 471−475.
Schirmer, T., Keller, T. A., Wang, Y.-F., & Rosencusch, J. P. (1995) *Science 267*, 512−514.
Weiss, M. S., Abele, U., Weckesser, J., Welte, W., Schiltz, E., & Schulz, G. E. (1991) *Science 254*, 1627−1630.

BI971232M